Journal of Power Sources 196 (2011) 4337–4341

Contents lists available at ScienceDirect

Journal of Power Sources

journal homepage: www.elsevier.com/locate/jpowsour

Short communication

Ethanol and CO electro-oxidation with amorphous alloys as electrodes

T.C. Blanco*, A.R. Pierna, J. Barroso

Dpto. de Ingeniería Química y del Medio Ambiente, Universidad del País Vasco (UPV-EHU), Plaza de Europa 1, 20018 San Sebastián, Spain

ARTICLE INFO

Article history:
Received 30 July 2010
Received in revised form 9 December 2010
Accepted 10 December 2010
Available online 21 December 2010

Keywords:
Ethanol
Electro-oxidation
DEFC
Amorphous alloys

ABSTRACT

In recent years the interest in the use of ethanol as fuel in direct ethanol fuel cells (DEFCs) has increased. Ethanol is less toxic than methanol and the bigger size of the molecule reduces the permeability through the electrolytic membrane. But, the use of this fuel with platinum catalysts leads to the acetaldehyde and acetic acid formation as main reaction products, so the electrical efficiency decreases. Furthermore, platinum shows an important susceptibility to CO poisoning which is formed during the ethanol electro-oxidation.

The aim of this work is the study of the electro-catalytic behaviour of ethanol and CO electro-oxidation reaction with amorphous alloys, obtained by mechanical alloying technique. $Ni_{59}Nb_{40}Pt_{0.6}Pd_{0.4}$, $Ni_{59}Nb_{40}Pt_{0.6}Rh_{0.4}$ and $Ni_{59}Nb_{40}Pt_{0.6}Rh_{0.2}Ru_{0.2}$ compositions were studied. The bi-catalytic alloys show a similar behaviour for the ethanol electro-oxidation. In comparison to these, the current density towards ethanol oxidation decreases with the presence of Ru, although the tri-catalytic electrode shows the best tolerance to CO, with a lower surface coverage compared to other studied.

© 2010 Elsevier B.V. All rights reserved.

1. Introduction

Nowadays, oil and its products are the main power sources worldwide. The high power demand versus an unstable supply generates continuous fluctuations in crude oil prices. This fact and the contribution of these fuels to climate change are the main reasons to search for alternative power sources. Polymer electrolyte membrane fuel cells (PEMFCs) are promising candidates for transportation applications and portable power sources. These systems use hydrogen as fuel and work at low temperatures, but pure hydrogen is difficult to produce and shows storage and distribution limitations. For this reason, a number of recent works are focused on the study of electro-catalytic oxidation of small organic molecules such as methanol and ethanol, due to their advantages compared to hydrogen. The lack of methanol availability, whose production is limited, has generated a growing interest in the use of ethanol as an alternative. Ethanol is less toxic than methanol, shows a lower permeability through the membrane used as electrolyte and could provide a higher power density, with the exchange of twelve electrons per molecule compared to the six electrons exchanged during the complete oxidation of methanol.

The platinum appears to be the most active and stable noble metal for the oxidation of such fuels in acid media, although it shows an important susceptibility to CO poisoning, which is formed during the electro-oxidation process, and it is usually combined with other metals to improve the catalyst effectiveness. Nevertheless, the use of ethanol in DEFCs shows an additional problem; the C–C bond cleavage is required for complete oxidation of the molecule to CO_2. So far the efficiency in the C–C bond activation in ethanol oxidation is quite low, and partial oxidation of fuel occurs with acetaldehyde and acetic acid formation as main products. This fact decreases the electrical efficiency of the process and the reaction mechanism is complicated. All species involved in the electro-oxidation reaction are unknown, but some authors [1–3] propose a general mechanism, that can be summarized in two steps. The first one is the ethanol adsorption and dissociation on Pt catalyst generating several adsorbed intermediates, which are oxidized to generate acetaldehyde, at low potentials. The acetaldehyde formed can be readsorbed over the surface to form acetyl species, which are oxidized to CO. The second step requires water molecules dissociation and oxidation, which occurs at higher potentials on Pt sites. In the presence of OH species on the electrode surface, the CO formed during previous steps can be finally oxidized to CO_2 (1), but these species can also react with acetyl radical and acetic acid is formed (2).

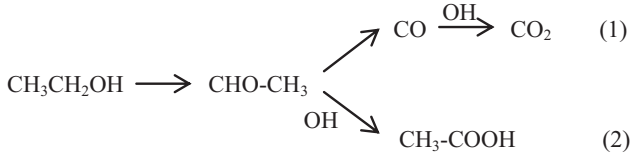

Nature and structure of the electrode material, directly affect the adsorption mode and kinetics of the reaction, and control the for-

* Corresponding author. Tel.: +34 943017127; fax: +34 943017131.
E-mail addresses: tamara.carballo@ehu.es (T.C. Blanco), iapropia@sp.ehu.es (A.R. Pierna).

0378-7753/$ – see front matter © 2010 Elsevier B.V. All rights reserved.
doi:10.1016/j.jpowsour.2010.12.018

mation of adsorbed intermediates, determining the oxidation end products. Thus, a better understanding of reaction mechanisms and development of new catalysts or changes to the platinum catalyst would improve the performance of DEFCs.

Previous studies showed an important catalytic activity of Pd in the hydrogen oxidation in acid media [4,5] and ethanol oxidation in alkaline media [6–8], besides achieving high CO tolerance with PtPd combination [9,10]. In addition, according to some authors [11–15], the PtRh combination increases the current density towards ethanol electro-oxidation, with higher efficiency of the process, compared with the same values obtained on Pt catalyst. When Rh is present as co-catalyst, the results showed higher CO_2/acetic acid ratio, so its addition increases the capability for C–C bond cleavage. Finally, it is widely known that the PtRu combination improves the kinetics of CO oxidation in comparison to Pt as single catalytic metal, due to a bi-functional mechanism [16–19]. Ruthenium is able to provide OH species at lower potential than for the case of Pt, with a significant reduction of the poisoning when this metal is present.

Most of the electrochemical works are carried out on metal–metal glasses, but not many are focused on NiNb based amorphous alloys. These metals, alloyed with platinum as catalyst and other metals as co-catalysts are used as anode materials for electrochemical treatment of toxic compounds, and for its application in fuel cells [20,21]. The amorphous state is more active than crystalline, with a greater density of active surface area. It also reduces the amount of platinum and, therefore, the overall cost of the catalyst.

In the present paper, catalytic activities of $Ni_{59}Nb_{40}Pt_{0.6}Pd_{0.4}$, $Ni_{59}Nb_{40}Pt_{0.6}Rh_{0.4}$ bi-catalytics and $Ni_{59}Nb_{40}Pt_{0.6}Rh_{0.2}Ru_{0.2}$ tri-catalytic alloys in ethanol and CO electro-oxidation were studied, via cyclic voltammetry, CO striping and chronoamperometry techniques.

2. Experimental

Preparation of the alloys used as catalyst was achieved by mechanical alloying technique during 40 h in a Restch PM 400 planetary ball mill. The metal elements were placed in a stainless steel vial with balls of the same material in a ratio of 1:4. The obtained alloys were characterized by differential scanning calorimetry (DSC), X-ray diffraction (XRD) and energy dispersive X-ray microanalysis (EDX) of images obtained by scanning electron microscopy (SEM). DSC measurements were carried out in a DSC 2920 Modulated system (TA instruments) with a standard cell model 2920 MDSC. For XRD experiments, a Philips X'Pert Pro powder diffractometer, working with CuKα radiation (λ = 1.54 Å) was used and the obtained patterns were normalized in the high q-range, where the intensity cannot vary between the different samples owing to the very short structural distances, which are responsible for the scattering in this region. A scanning electron microscope JEOL JSM-6400 with EDX microanalysis (Link eXL II Oxford) and Wavelength Dispersive X-ray (WDX) JEOL, were used to take and analyze the SEM images.

Carbon paste electrodes were made by hand-mixing each alloy with glassy carbon powder and paraffin. All catalysts were activated by immersion in analytical grade HF 48% solution for 10 s at room temperature and rinsed out with distilled water. Previous studies have concluded [22] that the surface of these amorphous alloys consists mainly of nickel and niobium oxides, metallic nickel and metallic niobium. After the HF treatment superficial oxides are removed and the surface is mainly composed of Pt and co-catalyst elements, so the chemical activation generates active sites on the electrode surface. Besides, a porous surface is obtained, enhancing the effective reaction area [23].

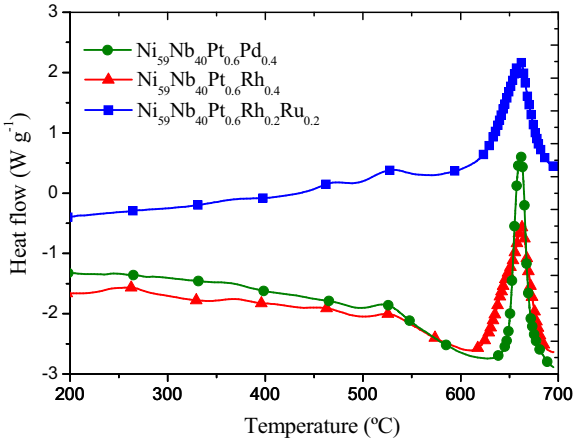

Fig. 1. Thermograms for $Ni_{59}Nb_{40}Pt_{0.6}Pd_{0.4}$, $Ni_{59}Nb_{40}Pt_{0.6}Rh_{0.4}$ and $Ni_{59}Nb_{40}Pt_{0.6}Rh_{0.2}Ru_{0.2}$ alloys, obtained at a constant heating rate of 10 °C min^{-1}, in N_2 atmosphere.

In order to compare the activities of the different catalysts, current density values obtained in the electrochemical experiments for the ethanol oxidation were normalized by the electrochemical active surface (EAS). Cyclic voltammetry test was performed in 0.1 M $HClO_4$ electrolytic solution and the EAS was determined using the coulombic charge for the hydrogen adsorption–desorption.

The electrochemical measurements were performed in a potentiostat/galvanostat (Solartron 1480 Multistat system) using a single flow cell with three electrodes: the working electrode, graphite as counter electrode and a commercial Ag/AgCl electrode as reference.

3. Results and discussion

3.1. Alloys characterization

The amorphous nature of the alloys was confirmed by DSC and XRD experiments. The DSC measurements were carried out in N_2 atmosphere at a heating rate of 10 °C min^{-1}. Fig. 1 shows the thermograms obtained for each of the alloys. A broad peak with positive heat flow can be observed around 662 °C, which indicates the development of an exothermic process ($\Delta H < 0$). Therefore, this peak is associated with the crystallization of the amorphous phase present in different alloys. On the other hand, Fig. 2 shows the X-ray diffraction patterns of amorphous alloys. Crystalline materials shows very narrow peaks during the X-ray diffractogram. The presence of the first peak (Fig. 2) is due to the supporting material and the broader second peak indicates the amorphous state of the alloys [16]. However, some single crystals may appear on the top surface of the alloys, which are dissolved by the pre-treatment with HF, exposing the inner amorphous structure [22].

The composition and homogeneity of the alloys were studied by energy dispersive X-ray microanalysis (EDX) of images obtained by scanning electron microscopy (SEM). This non destructive technique allows to look the field that is being analyzed and to obtain images of this. The analysis is carried out point to point and it is necessary to perform multiple measurements in order to decrease the error. Table 1 shows the average results obtained in atomic percentage for the elements of the bi-catalytic alloys. On the other hand, Table 2 shows the same results for the tri-catalytic alloy.

3.2. Ethanol electro-oxidation

It can be clearly observed in Fig. 3 that there are three oxidation peaks for ethanol electro-oxidation. According to the general reaction mechanism proposed, at low potentials, acetaldehyde is

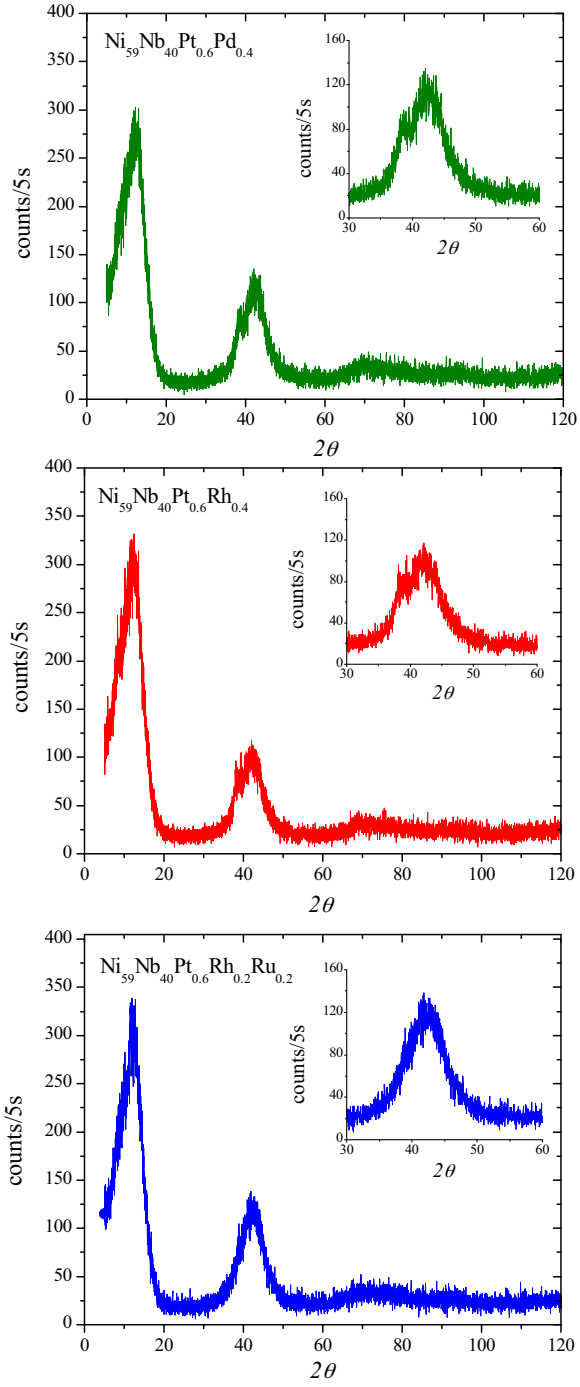

Fig. 2. X-ray diffraction patterns of $Ni_{59}Nb_{40}Pt_{0.6}Pd_{0.4}$, $Ni_{59}Nb_{40}Pt_{0.6}Rh_{0.4}$ and $Ni_{59}Nb_{40}Pt_{0.6}Rh_{0.2}Ru_{0.2}$ alloys.

Table 1
Average values obtained by EDX microanalysis for the elements of bi-catalytic alloys.

	Composition (at.%)			
	Ni	Nb	Pt	Pd
Theoretical value	59	40	0.6	0.4
Experimental	58.99	40.05	0.58	0.38
	Composition (at.%)			
	Ni	Nb	Pt	Rh
Theoretical value	59	40	0.6	0.4
Experimental	59.06	39.92	0.57	0.45

Table 2
Average values obtained by EDX microanalysis for the elements of tri-catalytic alloy.

	Composition (at.%)				
	Ni	Nb	Pt	Rh	Ru
Theoretical value	59	40	0.6	0.2	0.2
Experimental	59.08	39.87	0.66	0.21	0.18

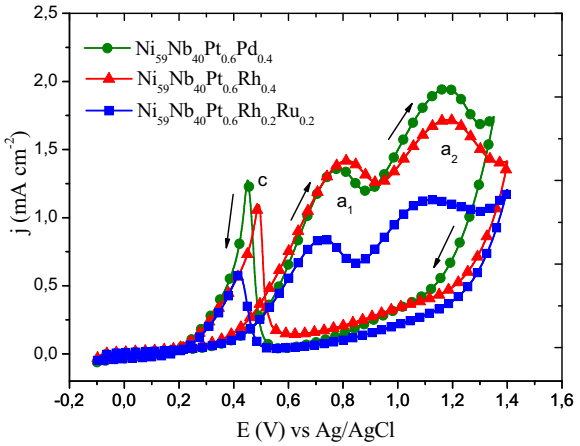

Fig. 3. Cyclic voltammograms obtained in 0.1 M $HClO_4$ and 1 M EtOH at 50 mV s^{-1} and 25 °C.

obtained as main product. At higher potentials, when OH species are present on the electrode surface, acetic acid is the main product formed. Therefore, the first anodic peak in Fig. 3 (a_1) could be associated to the acetaldehyde production; the second anodic peak (a_2) can be due to the acetic acid production and, finally, the current density of the anodic peak during the cathodic scan (c) could be associated with CO_2 generation. This last peak appears at the same potential values at which the CO electro-oxidation occur during the stripping experiments showed in Fig. 4.

If the catalytic activity is compared, the current density obtained decreases with the presence of Ru in the tri-catalytic alloy. The bi-catalytic alloys show a similar behaviour, although the ethanol electro-oxidation begins at a lower potential for the $Ni_{59}Nb_{40}Pt_{0.6}Rh_{0.4}$ electrode.

3.3. CO electro-oxidation

Fig. 4 shows the comparison of catalyst activities for CO selective oxidation as stripping voltammograms of saturated CO adlayer adsorbed at 0.04 V on the surface of each electrode.

Previous studies [18,19] showed a CO oxidation peak at 0.55 V when $Ni_{59}Nb_{40}Pt_1$ catalyst is used. Table 3 shows the potential (E_p) and peak area values obtained for $Ni_{59}Nb_{40}Pt_{0.6}Pd_{0.4}$, $Ni_{59}Nb_{40}Pt_{0.6}Rh_{0.4}$ and $Ni_{59}Nb_{40}Pt_{0.6}Rh_{0.2}Ru_{0.2}$ electrodes. In all cases, the peak potential for the maximum amount of oxidized CO shifts towards negative values, so the addition of co-catalyst improves the catalytic behaviour in CO electro-oxidation in comparison with $Ni_{59}Nb_{40}Pt_1$. An important shift is observed for $Ni_{59}Nb_{40}Pt_{0.6}Rh_{0.4}$ and $Ni_{59}Nb_{40}Pt_{0.6}Rh_{0.2}Ru_{0.2}$. Less energy is required for the reactivation of the catalytic surface compared with

Table 3
Electrochemical characteristics for CO electro-oxidation.

	E_p (V)	Area (cm^2)
$Ni_{59}Nb_{40}Pt_{0.6}Pd_{0.4}$	0.50	5.33
$Ni_{59}Nb_{40}Pt_{0.6}Rh_{0.4}$	0.40	4.93
$Ni_{59}Nb_{40}Pt_{0.6}Rh_{0.2}Ru_{0.2}$	0.41	1.02

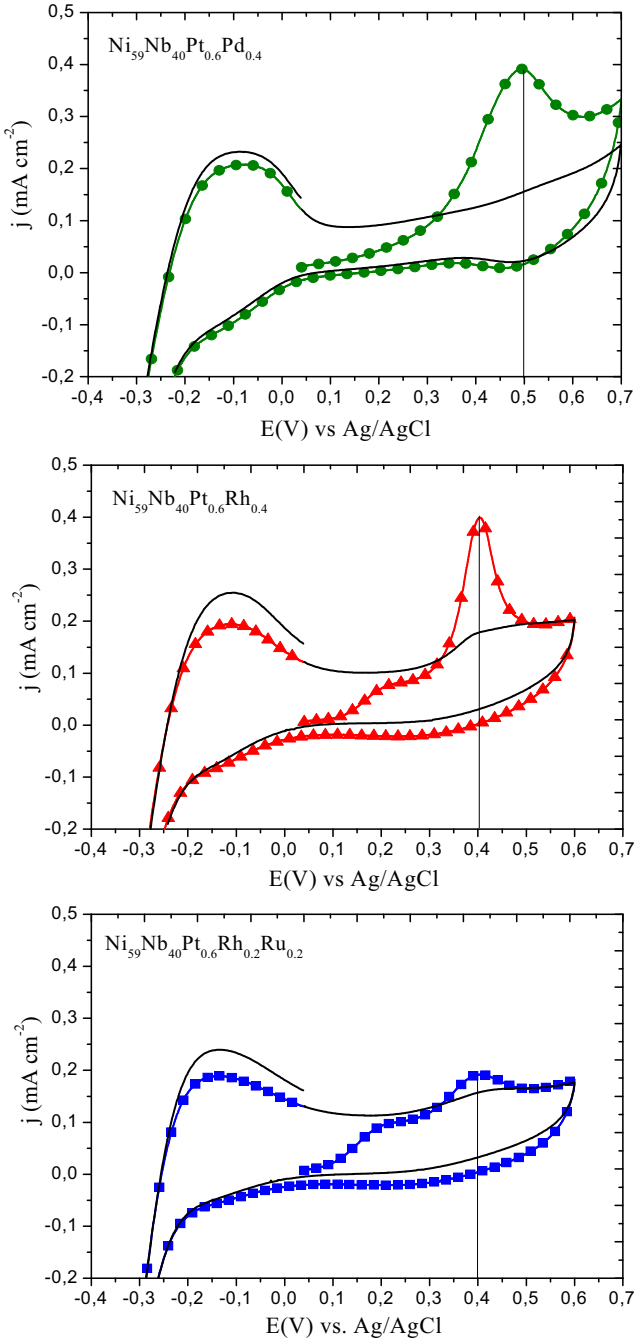

Fig. 4. CO stripping obtained in 0.1 M $HClO_4$ saturated solution, 0.04 V adsorption potential, 50 mV s^{-1}, 25 °C.

$Ni_{59}Nb_{40}Pt_{0.6}Pd_{0.4}$ and the CO oxidation occurs in the best range of working potential for a DEFC, between 0.4 and 0.6 V vs. NHE (0.20 and 0.40 V approx. vs. Ag/AgCl) [3].

The most significant difference between the studied catalysts concerns the values of peak area obtained by integrating the oxidation peak, assuming a 420 μC cm^{-2} load for a CO monolayer adsorbed on Pt. These values indicate the amount of CO that reacts, which has been pre-adsorbed on the electrode surface. According to the results, the order for the CO coverage on the different catalysts surface is the following: $Ni_{59}Nb_{40}Pt_{0.6}Rh_{0.2}Ru_{0.2} < Ni_{59}Nb_{40}Pt_{0.6}Rh_{0.4} < Ni_{59}Nb_{40}Pt_{0.6}Pd_{0.4}$.

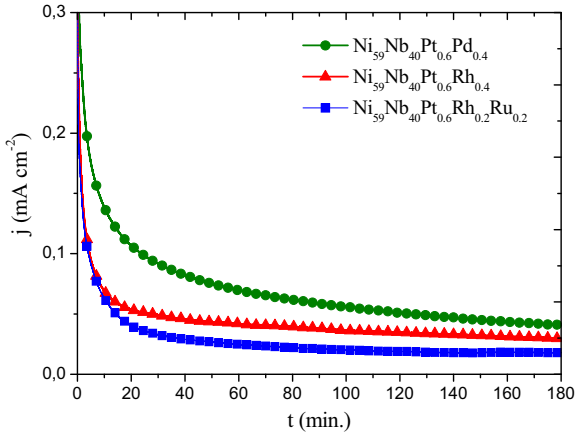

Fig. 5. Chronoamperograms obtained in 1 M $HClO_4$ and 1 M EtOH, 25 °C.

3.4. CO tolerance during ethanol electro-oxidation

As it can be observed in Fig. 5, current transients were measured holding the different catalysts at the first anodic peak potential in order to study the CO tolerance. In the first few seconds, the current measured for the $Ni_{59}Nb_{40}Pt_{0.6}Rh_{0.2}Ru_{0.2}$ catalyst dropped faster than that for the other catalysts. But, if the linear decay of the current density variation is studied at longer times, the tri-catalytic electrode shows the smaller slope compared to results obtained for the bi-catalytic electrodes.

The linear decay of the current densities at long periods of time may be characterized by the poisoning rate [24]:

$$\delta = \left| \frac{100}{j_0} \times \frac{dj}{dt} \right| (\%s^{-1})$$

where dj/dt is the slope of the linear portion of the current decay, and j_0 is the current at the start of polarisation back extrapolated from the linear current decay. From this equation a poisoning rate of 0.271% s^{-1}, 0.184% s^{-1} and 0.156% s^{-1} for $Ni_{59}Nb_{40}Pt_{0.6}Pd_{0.4}$, $Ni_{59}Nb_{40}Pt_{0.6}Rh_{0.4}$ and $Ni_{59}Nb_{40}Pt_{0.6}Rh_{0.2}Ru_{0.2}$ catalysts is obtained, respectively. The CO tolerance improves in the presence of Ru. The removal of CO formed during ethanol electro-oxidation, requires the presence of OH species on the electrode surface. Water molecules dissociation to form these species can occur on both platinum (3) and ruthenium sites (4), however in the case of ruthenium this take place at lower potentials. After that, CO which is formed during previous steps can be oxidized to CO_2 by interaction with OH species formed on Pt sites (5) or Ru sites (6).

$$Pt + H_2O \rightarrow Pt(OH)_{ads} + H^+ + e^- \quad (3)$$

$$Ru + H_2O \rightarrow Ru(OH)_{ads} + H^+ + e^- \quad (4)$$

$$Pt(CO)_{ads} \rightarrow Pt(OH)_{ads} \rightarrow Pt + CO_2 + H^+ + e^- \quad (5)$$

$$Pt(CO)_{ads} \rightarrow Ru(OH)_{ads} \rightarrow Pt + Ru + CO_2 + H^+ + e^- \quad (6)$$

According to the results, the order for the CO tolerance is the following: $Ni_{59}Nb_{40}Pt_{0.6}Pd_{0.4} < Ni_{59}Nb_{40}Pt_{0.6}Rh_{0.4} < Ni_{59}Nb_{40}Pt_{0.6}Rh_{0.2}Ru_{0.2}$.

4. Conclusions

The addition of co-catalysts reduces the amount of platinum in the electrode and improves its behaviour for CO electro-oxidation.

$Ni_{59}Nb_{40}Pt_{0.6}Pd_{0.4}$ and $Ni_{59}Nb_{40}Pt_{0.6}Rh_{0.4}$ are the most effective catalyst in the ethanol electro-oxidation, whereas the current density decreases for the tri-catalytic electrode of $Ni_{59}Nb_{40}Pt_{0.6}Rh_{0.2}Ru_{0.2}$ composition. Between the bi-catalytic electrodes, $Ni_{59}Nb_{40}Pt_{0.6}Rh_{0.4}$ shows a higher catalytic activity in CO electro-oxidation, due to the maximum amount of CO which is oxidized at lower potentials and the surface coverage is also lower. Besides, the CO oxidation peak potential for $Ni_{59}Nb_{40}Pt_{0.6}Rh_{0.4}$ is in the best working potential range for a DEFC (between 0.2 and 0.4 V vs. Ag/AgCl).

It can be concluded that the $Ni_{59}Nb_{40}Pt_{0.6}Rh_{0.4}$ is the most effective for its use as anode in a DEFC.

Acknowledgements

The authors gratefully acknowledge financial support of the Basque Government (IT515-10), Diputación Foral de Guipúzcoa (94/2008) and MEC (CTQ2006-13163/BQU).

References

[1] F.C. Simoes, D.M. dos Anjos, F. Vigier, J.-M. Léger, F. Hahn, C. Coutanceau, E.R. González, G. Tremiliosi-Filho, A.R. de Andrade, P. Olivi, K.B. Kokoh, J. Power Sources 167 (2007) 1–10.
[2] F. Vigier, S. Rousseau, C. Coutanceau, J.-M. Léger, C. Lamy, Top. Catal. 40 (2006) 111–121.
[3] S. Rousseau, C. Coutanceau, C. Lamy, J.-M. Léger, J. Power Sources 158 (2006) 18–24.
[4] E.N. Muhamad, T. Takeguchi, G. Wang, Y. Anzai, W. Ueda, J. Electrochem. Soc. 156 (1) (2009) B32–B37.
[5] S.A. Grigoriev, E.K. Lyutikova, S. Martemianov, V.N. Fateev, Int. J. Hydrogen Energy 32 (2007) 4438–4442.
[6] G. Cui, S. Song, P. Shen, A. Kowal, C. Bianchini, J. Phys. Chem. C 113 (2009) 15639–15642.
[7] X. Wang, W. Wang, Z. Qi, C. Zhao, H. Ji, Z. Zhang, Electrochem. Commun. 11 (2009) 1896–1899.
[8] F. Hu, C. Chen, Z. Wang, G. Wei, P. Shen, Electrochim. Acta 52 (2006) 1087–1091.
[9] A.C. Garcia, V.A. Paganin, E.A. Ticianelli, Electrochim. Acta 53 (2008) 4309–4315.
[10] D.C. Papageorgopoulos, M. Keijzer, J.B.J. Veldhuis, F.A. de Bruijn, J. Electrochem. Soc. 149 (11) (2002) A1400–A1404.
[11] Q. Yuan, Z. Zhou, J. Zhuang, X. Wang, Chem. Mater. 22 (2010) 2395–2402.
[12] K. Bergamaski, E. González, F. Carlos Nart, Electrochim. Acta 53 (2008) 4396–4406.
[13] F.H.B. Lima, D. Profeti, W.H. Lizcano-Valbuena, E.A. Ti-cianelli, E.R. Gonzáles, J. Electroanal. Chem. 617 (2008) 121–129.
[14] F.H.B. Lima, E.R. González, Electrochim. Acta 53 (2008) 2963–2971.
[15] R.T.S. Oliveira, M.C. Santos, B.G. Marcussi, S.T. Tanimoto, L.O.S. Bulhoes, E.C. Pereira, J. Power Sources 157 (2006) 212–216.
[16] J. Barranco, A.R. Pierna, J. New Mater. Electrochem. Syst. 12 (2009) 69–76.
[17] J. Barranco, A.R. Pierna, J. Non-Crystall. Solids 354 (2008) 153–5155.
[18] J. Barranco, A.R. Pierna, J. Power Sources 169 (2007) 71–76.
[19] J. Barranco, A.R. Pierna, J. Non-Crystall. Solids 353 (2007) 851–854.
[20] M. Sistiaga, A.R. Pierna, J. Non-Crystall. Solids 329 (2003) 184–187.
[21] A.R. Pierna, M. Sistiaga, C. Navascués, A. Lorenzo, J. Non-Crystall. Solids 287 (2001) 432–436.
[22] M. Sistiaga, A. Cuesta, A.R. Pierna, C. Gutiérrez, Surf. Sci. 410 (1998) 312–320.
[23] R. González-Huerta, I. Guerra-Martínez, J. Santiago López, A.R. Pierna, O. Solorza-Feria, J. New Mater. Electrochem. Syst. 13 (2010) 171–176.
[24] J. Jiang, A. Kucernak, J. Electroanal. Chem. 543 (2003) 187–199.